Showcasing the study of the CH₃-induced nucleation mechanism for epitaxial growth of bilayer graphene by Prof. Pei Zhao at Laboratory of Graphene Mechanics (LogM), Institute of Applied Mechanics and Key Laboratory of Soft Machines and Smart Devices of Zhejiang Province, Zhejiang University.

Epitaxial nucleation of CVD bilayer graphene on copper

Experimental study and first-principles calculations of the chemical vapor deposition (CVD) nucleation process for Bernal-stacked bilayer graphene (BLG) growth on copper using ethanol precursor demonstrate that a carefully adjusted flow rate of ethanol yields a uniform BLG film with a surface coverage of nearly 90% and Bernal-stacking ratio of nearly 100% on ordinary flat copper substrates. Also, the epitaxial nucleation of the second layer is mainly due to the active CH₃ radicals decomposed from ethanol with the presence of the monolayer-graphene-covered copper surface.

ROYAL SOCIETY OF CHEMISTRY
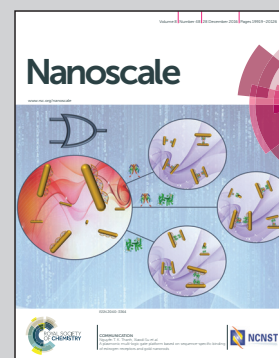
www.rsc.org/nanoscale

Nanoscale

PAPER

CrossMark
‹ click for updates

Epitaxial nucleation of CVD bilayer graphene on copper†

Yenan Song,[a] Jianing Zhuang,[b] Meng Song,[c] Shaoqian Yin,[a] Yu Cheng,[a] Xuewei Zhang,[a] Miao Wang,[c] Rong Xiang,[d] Yang Xia,[e] Shigeo Maruyama,[d] Pei Zhao,*[a] Feng Ding*[b] and Hongtao Wang*[a]

Bilayer graphene (BLG) has emerged as a promising candidate for next-generation electronic applications, especially when it exists in the Bernal-stacked form, but its large-scale production remains a challenge. Here we present an experimental and first-principles calculation study of the epitaxial chemical vapor deposition (CVD) nucleation process for Bernal-stacked BLG growth on Cu using ethanol as a precursor. Results show that a carefully adjusted flow rate of ethanol can yield a uniform BLG film with a surface coverage of nearly 90% and a Bernal-stacking ratio of nearly 100% on ordinary flat Cu substrates, and its epitaxial nucleation of the second layer is mainly due to the active CH_3 radicals with the presence of a monolayer-graphene-covered Cu surface. We believe that this nucleation mechanism will help clarify the formation of BLG by the epitaxial CVD process, and lead to many new strategies for scalable synthesis of graphene with more controllable structures and numbers of layers.

Introduction

Bilayer graphene (BLG), a two-dimensional material consisting of two atomic layers of carbon honeycomb lattices, has emerged as a promising candidate for next-generation electronic applications, especially when it exists in the Bernal-(AB-) stacked form, due to the fact that a bandgap of ~250 meV can be developed near its Dirac points by applying a vertical electric field across the two layers.[1,2] However, by far the large-scale production of Bernal-stacked bilayer graphene remains a challenge. Although in the past few years there have been many exciting achievements in the synthesis of large-size and high-quality monolayer graphene (MLG) using the chemical vapor deposition (CVD) method on Cu substrates,[3–5] developing a practical and scalable method to obtain Bernal-stacked BLG is still a hot pursuit for future applications.

Previous reports have shown that the CVD synthesis of BLG on Cu is possible if more active carbon precursors or designed CVD processes are adopted,[6–15] and the key point of these modifications to ordinary CVD is to overcome the self-limiting nature of MLG on Cu. Usually, the second layer of BLG grows underneath the first-grown layer with shared nucleation sites, especially when methane is used as the carbon precursor, as evidenced from the isotope-labeling results,[10,11] therefore the growth of these second nuclei will be strongly restricted and stopped by the expansion of their covered first layer. Moreover, because the nucleation of graphene grains is a super-saturation process of carbon on the defective Cu surface, BLG growth from below also suggests a possible non-Bernal-stacking between the two graphene layers.[11] On the other hand, several reports also demonstrated a layer-by-layer epitaxial growth of BLG by CVD,[12–15] which has gradually become a topic of significant interest. Epitaxial CVD growth can yield relatively more uniform BLG with a high surface coverage and Bernal-stacking ratio, usually nearly 100%. During this growth, the second graphene layer grows on top of the first layer, and it is generally believed that the van der Waals (vdWs) force plays an important role in forming this high Bernal-stacking ratio.[13–15] However, many crucial aspects of the epitaxial CVD growth of BLG are still not fully understood and require additional investigation, among which the most important and fundamental one is the nucleation process of the second graphene layer on the formed first layer, *i.e.*, how the new graphene layer nucleates on top on the formed graphene in the absence of a direct contact with the catalytic Cu surface.

[a]*Institute of Applied Mechanics and Key Laboratory of Soft Machines and Smart Devices of Zhejiang Province, Zhejiang University, Hangzhou 310012, P. R. China. E-mail: peizhao@zju.edu.cn, htw@zju.edu.cn*
[b]*Institute of Textiles and Clothing, Hong Kong Polytechnic University, Kowloon, Hong Kong, China. E-mail: feng.ding@polyu.edu.hk*
[c]*Department of Physics, Zhejiang University, Hangzhou 310012, P. R. China*
[d]*Department of Mechanical Engineering, The University of Tokyo, Bunkyo-ku, Tokyo 113-8656, Japan*
[e]*Institute of Microelectronics, Chinese Academy of Science, Beijing 100029, P. R. China*
†Electronic supplementary information (ESI) available: Supplementary figures. See DOI: 10.1039/c6nr04557j

To this end, we present an experimental and first-principles calculation study of the epitaxial CVD nucleation process for Bernal-stacked BLG growth on Cu using ethanol as the precursor. Results show that a carefully adjusted flow rate of ethanol can yield a uniform BLG film with a surface coverage of nearly 90% and a Bernal-stacking ratio of nearly 100% on ordinary flat Cu substrates, and its epitaxial nucleation of the second layer is mainly due to the active CH_3 radicals with the presence of a MLG-covered Cu surface. We believe that this nucleation mechanism will help clarify the formation of BLG by the epitaxial CVD process, and lead to many new strategies for scalable synthesis of graphene with more controllable structures and numbers of layers.

Results and discussion

Zhao *et al.* have previously reported that the growth of Bernal-stacked BLG is an equilibrium process using ethanol as the carbon precursor,[15] but they used a folded Cu enclosure as the growth substrate, and uniform BLG was only obtained on the inside surface of the enclosure. This special substrate structure makes it difficult not only for the scaling-up synthesis, but also for the understanding of a more detailed growth mechanism. In our approach, we chose the ethanol-based CVD system to grow BLG but attempted to reproduce its results on flat Cu, which as we show later will largely help understand its nucleation mechanism. Moreover, a flat Cu foil significantly enlarges the size of a BLG film that can be grown in the CVD furnace when it is rolled up into a cylinder. As shown in the schematic image of the CVD system in Fig. S1 in the ESI,† we used the release valve of Ar gas to control its pressure to 0.5 atm. On the other hand, the ethanol tank was maintained at 19 °C, which resulted in a saturated vapor pressure of 0.53 kPa for ethanol. Therefore, the pressure ratio between Ar and ethanol was approximately 10 : 1, and this ratio provided the detailed ethanol partial pressures that were used in the CVD experiments. Moreover, Ar also behaved as the carrying and diluting gas for ethanol in the experiments. The uniform and scalable BLG film was obtained on flat Cu foil under optimal conditions (20 sccm Ar/ethanol, 3 hour growth, partial pressure of ethanol is ~3 Pa), as shown in Fig. 1a. Fig. 1b shows a typical optical microscopy (OM) image of the BLG film after being transferred onto a Si substrate with a 300 nm SiO_2 layer, and the sample uniformity can be evaluated by its color contrast. No areas with different contrasts are apparent, indicating that the layer number is uniform. The scanning electron microscopy (SEM) image in Fig. 1c also demonstrates the uniformity of the as-grown graphene on the Cu foil. The layer number of the graphene film is confirmed by Raman spectroscopy, as shown by the representative Raman spectra in Fig. 1d, which all show features of Bernal-stacked BLG such as a 2D-band (~2690 cm^{-1}) to G-band (~1582 cm^{-1}) intensity ratio (I_{2D}/I_G) of ~1, and an asymmetric 2D-band with a full width at half-maximum (FWHM) value of ~45–60 cm^{-1}.[16] Fig. 1e shows the select area electron diffraction (SAED)
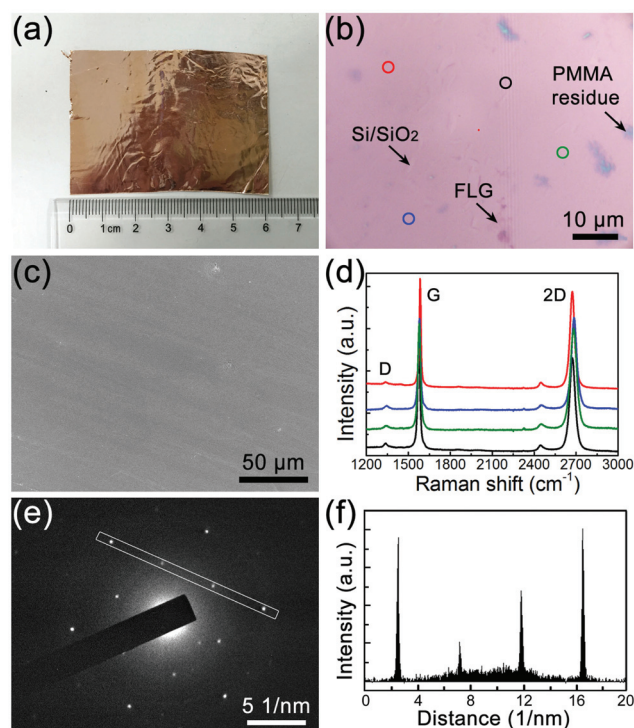

Fig. 1 (a) Photograph of a Cu foil after the CVD growth of BLG under optimal conditions for 3 hours. (b) OM image of a BLG film on a Si substrate with a 300 nm SiO_2 layer. (c) SEM image of the as-grown BLG film on a Cu foil. (d) Typical Raman spectra of BLG measured from four random spots in (b). (e) SAED pattern of a BLG domain, which shows a clear 6-fold symmetry. (f) Spot intensities in the white box in (e).

pattern of a BLG domain using transmission electron microcopy (TEM), and only a single set of 6-fold symmetric diffraction spots is observed. The corresponding spot intensities in Fig. 1f clearly demonstrate the Bernal-stacking structure of the BLG samples.[15]

The uniformity of these BLG samples can be further evaluated by the Raman contour maps of their I_G, I_{2D}/I_G, FWHM of the 2D-band, and the D-band to G-band intensity ratio (I_D/I_G), as shown in Fig. 2a–d, respectively. These Raman spectra were collected over a 4500 μm^2 with 30 × 30 scanning points. We chose the range of Raman I_{2D}/I_G from 0.7 to 1.3 and the FWHM of the 2D-band from 45 to 60 cm^{-1} to evaluate Bernal-stacked BLG quality.[15,17] The coverage of Bernal-stacked BLG, MLG and few-layer graphene (FLG) was determined to be ~89%, ~8% and ~3%, respectively, and no Raman features from twisted BLG were observed.[18] Fig. 2f shows the Raman spectra that are representative of MLG, BLG and FLG in the BLG sample.

We interrupted the CVD process to obtain more information of the growth, by stopping the Ar/ethanol flow after different growth periods. The SEM images of these results are presented in Fig. 3a. The flow rate of Ar/ethanol is maintained at 20 sccm, and the corresponding partial pressure of ethanol is ~3 Pa. After 3 min, many MLG islands are found to nucleate on the Cu surface, with typical sizes smaller than 5 μm. Most of these islands coalesce to achieve a coverage of ~70% of the
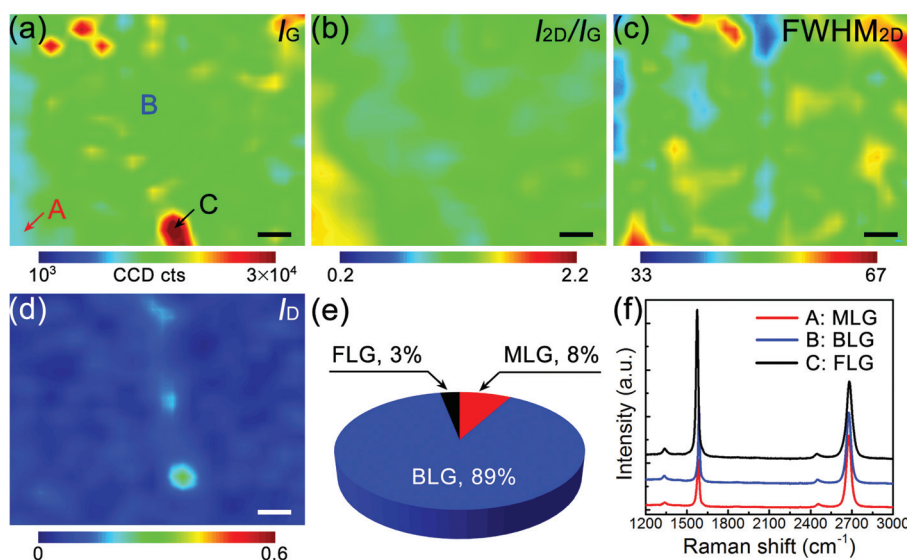
Fig. 2 Scanning Raman maps of ethanol-derived BLG on flat Cu for (a) I_G; (b) I_{2D}/I_G; (c) FWHM of the 2D-band; (d) I_D/I_G. Scale bars in (a–d): 10 μm. (e) Corresponding pie chart of graphene coverage for BLG, MLG, and FLG in the BLG film. (f) Raman spectra representative of MLG, BLG and FLG, measured from the regions indicated by red, blue, and black arrows in (a), respectively.
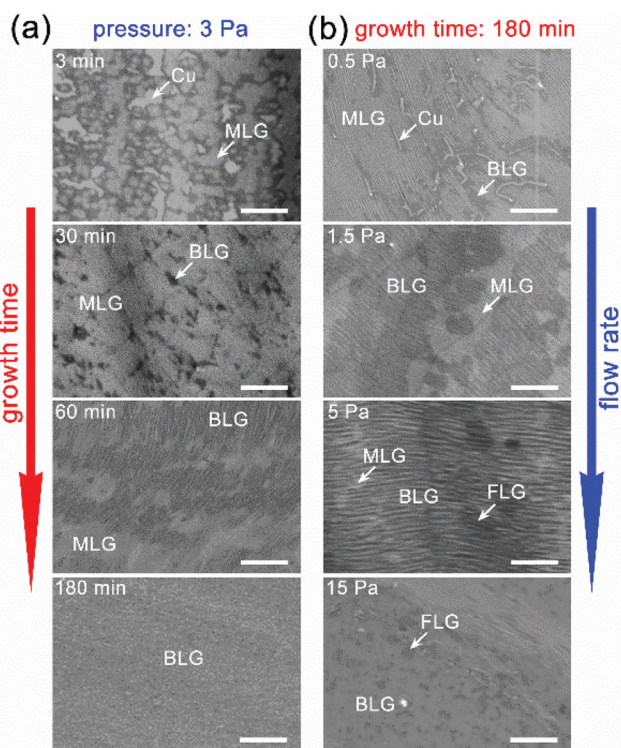

Fig. 3 (a) SEM images of BLG growth using a partial pressure of ethanol at 3 Pa with different growth periods of 3, 30, 60 and 180 min. (b) SEM images of graphene growth using different Ar/ethanol flow rates and the same growth time of 180 min, and the corresponding ethanol partial pressures are 0.5, 1.5, 5 and 15 Pa. Scale bars in (a) and (b): 5 μm.

Cu surface. After 30 min, MLG is completely formed and no unfilled gaps between islands are observed. The self-limiting growth stage of this MLG is maintained for a short time and

the nucleation of the second graphene layer starts soon. After 60 min, many new graphene islands appear and coalesce to form the second layer, with a total coverage of over 50% of the whole Cu/MLG surface. Moreover, it is visible that the graphene grain size of the secondly grown layer from ethanol is approximately 1 to 3 μm, significantly smaller than that from methane with equivalent pressure. The growth rate of the second layer is significantly reduced after 60 min and a continuous second layer is finally completed after 3 hours and achieves an equilibrium state (Fig. S2 in the ESI†).

Ethanol can affect the BLG growth on flat Cu in a more straightforward way, therefore it is necessary to investigate the relationship between the ethanol flow and the yield, as shown in Fig. 3b. Apparently, an appropriate partial pressure of ethanol is critical to obtain the best quality of BLG. When the partial pressure of ethanol is low, it yields MLG with unfilled gaps and randomly distributed BLG flakes, or a non-uniform graphene film with a discontinuous second layer. On the other hand, when the partial pressure of ethanol is high, graphene islands with more layers easily nucleate and expand, and finally yields a graphene film with more layers.

The previous BLG growth from ethanol has demonstrated that the growth follows a layer-by-layer epitaxy, in which the second layer grows atop the first one.[15] Although it uses Cu enclosures instead of flat Cu foils, we believe that this difference will not change this epitaxial growth mode. In the typical "growth-from-below" model, after the first graphene layer is completed, the catalytically active Cu surface and the diffusion channels from the graphene grain edges to below the grains both disappear, making it prohibitive to expand the graphene layers that are below the first layer.[3] The epitaxial growth mode of BLG in our experiments can also be confirmed by its time-dependent SEM images in Fig. 3, which clearly show that the

grains of the second graphene layer start to form after the full coalescence of the first layer, and keep expanding with a prolonged CVD time.

To reveal the nucleation mechanism of the epitaxial CVD growth of BLG on Cu, we performed a theoretical study using first-principles calculations. The calculations are based on the fact that the Cu surface can maintain its influence on graphene nucleation even after it is fully covered by a layer of graphene, evident from the experimental results that no second graphene layers can be grown on transferred MLG/SiO$_2$/Si substrates in an equivalent CVD environment (Fig. S3 in the ESI†). We use the basic forms of carbon radicals CH$_i$ (i = 0, 1, 2, 3) as possible fundamental bricks for the nucleation of a new graphene layer, together with the Cu(111) surface and the formed graphene layer(s) as the studied system. More detailed geometries of these systems are shown in Fig. S4 in the ESI.† The relative binding strength of these CH$_i$ radicals on the Cu(111)/graphene surfaces can be presented in terms of their binding energy E_b

$$E_b = E_{sub} + E_{CH_i} - E_{sys} \tag{1}$$

where E_{sub}, E_{CH_i}, and E_{sys} are the energies of the Cu(111)/graphene substrate, the CH$_i$ species, and the whole system, respectively. The total energy and binding energy data of E_{sub}, E_{CH_i}, E_{sys}, and E_b for these CH$_i$ on Cu(111)/graphene systems are summarized in Tables S1 and S2 in the ESI,† respectively. During the nucleation process, a strong binding energy between the CH$_i$ species and the substrate is needed. The calculation results demonstrate that the interactions between CH$_i$ and all Cu(111)/graphene substrates are in the form of chemical bonding, as shown in Fig. 4. For MLG nucleation on the Cu(111) surface, only radicals with a relatively stronger binding energy (E_b > 3.0 eV) contribute to the growth of the first graphene layer, as mentioned in our previous report.[19] For BLG nucleation, radicals of C, CH and CH$_2$ exhibit higher binding energies on Cu(111)/BLG than on Cu(111)/MLG

(Fig. 4a–c), indicating that once a second graphene layer is nucleated, these radicals prefer to immediately nucleate a third layer on top of it. On the other hand, the CH$_3$ radicals have a binding energy of ~1.07 eV on Cu(111)/MLG and a binding energy of ~0.34 eV on Cu(111)/BLG (Fig. 4d), and this weakened binding strength makes it possible for the CH$_3$ radicals to be adsorbed on a Cu/MLG surface and nucleate only the second layer but not together with the third one. What the above calculations highlight is the binding energy differences for different radicals on different substrates, aiming to identify the most active radicals that facilitate the growth process. Moreover, since one radical is small in size compared to the defective sites that are capable of nucleation, such as the grain boundary, step or edge, we believe that the bonding behavior of radicals should be similar to that on the flat Cu substrate.

This scenario of CH$_3$-assisted nucleation is consistent with the reports of Wassei et al.[12] and Yan et al.[13] in which they both proposed that alkyl radicals are the main contributors to the epitaxial nucleation of a new graphene layer. This adsorption process of CH$_3$ radicals on the first graphene layer can also be assisted by a trapping mediated process,[20] in which a scattered CH$_3$ radical can be trapped at the basal plane of the graphite surface for a short time at the environmental temperature much higher than its desorption temperature. This has been experimentally demonstrated by a Li-induced CH$_3$Cl dissociative reaction with graphite.[21] We believe that this nucleation mechanism can also be further extended to other epitaxial CVD growth systems for BLG.

The above discussion is based on the assumption that the metal substrate is dominated by the Cu(111) facet. Theoretically, the top layer atomic packing on a Cu(111) facet has a C_{6v} symmetry,[22] the same as graphene and therefore allows a highly oriented graphene synthesis. In the above BLG growth experiments, most graphene first layer domains are in the six-fold symmetry and therefore we believe that the substrate is dominated by Cu(111) facets. Moreover, because we are considering the growth of the second graphene layer on the top of the first one, the effect of the type of Cu facet must be minor. Therefore, we believe the main conclusion of this study can also be applied to other Cu facets.

Similar to ethanol, its thermal decomposition at high temperatures is not well understood yet. Ethanol may decompose via many energetically accessible product channels. Considering the bond energies of C–O and C–C, the following two reactions:

$$C_2H_5OH \rightarrow C_2H_4 + H_2O \tag{2}$$

$$C_2H_5OH \rightarrow CH_3 + CH_2OH \tag{3}$$
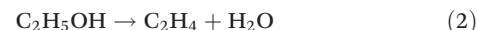
are expected to be the dominant channels.[23–28] Particularly, channel reaction (3) is a barrierless path. We calculated the thermal decomposition products of ethanol under our equivalent experimental conditions using the CHEMKIN-II software package, and show its time-dependent gas composition of ethanol in Fig. S5 in the ESI.† Approximately 97% of ethanol decomposes after 1 s, with various decomposition pro-
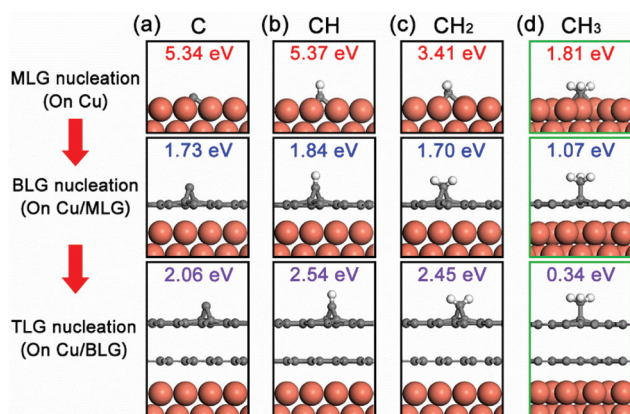

Fig. 4 Adsorption configurations and binding energies of (a) C monomer, (b) CH, (c) CH$_2$ and (d) CH$_3$ on top of the Cu surface, the Cu surface with MLG, and the Cu surface with BLG. Only the binding energies of CH$_3$ radicals are suitable for epitaxial nucleation of the second graphene layer.

ducts of C_2H_4, C_2H_2, CH_3, CH_2O, *etc*. Considering that radicals are much more active in graphene growth reactions than molecules, among all types of radicals CH_3 shows a molar fraction of ~0.26%, two and four orders of magnitude higher than those of CH_2 and CH, respectively, as shown in Fig. 5a. On the other hand, the thermal decomposition of methane is negligible at 1000 °C and can hardly generate any CH_i radicals for graphene growth (molar fractions: $CH_3 \sim 10^{-8}$, $CH_2 \sim 10^{-17}$, $CH \sim 10^{-28}$). This is also consistent with the self-limiting growth behavior for MLG when methane is used.

For other alkanes that can also thermally decompose with CH_3 radicals such as C_2H_6, Wassei *et al.* have shown that BLG with a coverage of up to 49% can be obtained. A previous report has shown that graphene layers can form on HOPG by CH_3 radicals depending on the defects, and the largest sticking probability of 10^{-6} was observed when the HOPG surfaces are prestructured with nanometer-sized etch pits.[29] Compared with C_2H_6, due to the decomposed products of H_2, H_2O, and/or other OH contained radicals, C_2H_5OH induces etching and regrowth sites in the firstly grown graphene layer,[15] which may also simultaneously behave as more possible CH_3 nucleation sites. This increases the nucleation probability of the new graphene layer, and results in a higher coverage of BLG. Moreover, besides generating CH_3 nucleation sites, the OH radicals also play an important role in accelerating the growth by lowering the energy barrier of carbon adatoms.[5]

We further consider the stability of each CH_i radical on a Cu/MLG surface. Fig. 5b shows the relative Gibbs free energies of species of each CH_i radical on Cu(111)/MLG as a function of the chemical potential of H (μ_H). It is found that the stability of CH_i highly depends on μ_H, and CH_3 is the dominating species in the regime of $\mu_H > -1.24$ eV. In our experiments, no H_2 is used and μ_H mainly depends on the thermally decomposed H from ethanol. However, because the final decomposition products of ethanol usually react with H atoms,[25–28] H atoms can hardly be generated in all ethanol decomposition channels and its chemical potential is close to 0, which prefers the nucleation of the second graphene layer by CH_3 radicals.

Based on this, we propose the nucleation mechanism of ethanol-based epitaxial CVD growth for BLG on Cu in Fig. 6. For the MLG, ethanol behaves similarly as methane,[30] and the C, CH, and CH_2 radicals catalyzed from ethanol by Cu contrib-
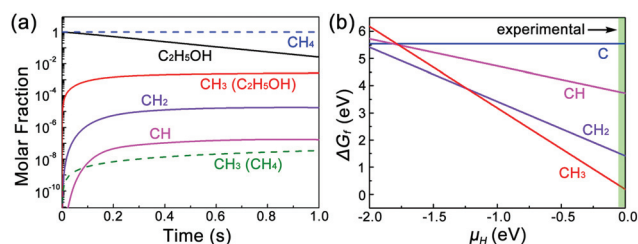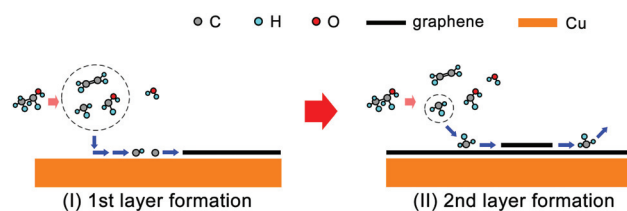

Fig. 6 Schematic of the possible mechanism for epitaxial CVD growth of BLG on Cu using ethanol as the carbon precursor.

ute the most to its nucleation and growth. After the MLG formation, the absence of a direct contact between ethanol and Cu makes it difficult to generate radicals of C, CH and CH_2, whose binding energies do not match the nucleation of only BLG as well. On the other hand, CH_3 radicals play a crucial role in nucleating the second graphene layer, not only because it is a product of thermally decomposed ethanol, but also because of its suitable binding energies on Cu/MLG and Cu/BLG.

Finally, it needs to be emphasized that after the grain nucleation of the second graphene layer by CH_3 radicals, the following carbon deposition process remains unclear. Although the C–H dissociation energy is calculated to be 480 kJ mol^{-1},[31] which makes it impossible for the direct dissociation of another C–H bond in the nucleated CH_3 radical, the actual energy barrier for CH_3 and H exchange is considerably lower and accessible at reaction temperatures.[32] Moreover, the OH radicals may also play some role in lowering the activation energy of the edge dehydrogenation, similar to that in an oxygen-assisted CVD growth for the centimeter-scale graphene single crystals.[5]

Conclusion

In conclusion, we demonstrate an experimental and first-principles calculation study of the epitaxial CVD growth for Bernal-stacked BLG on Cu using ethanol. The surface coverage of BLG in the sample is nearly 90% and the Bernal-stacking ratio is nearly 100%. Under an equilibrium CVD environment, the BLG growth exhibits two self-limiting processes for the two graphene layers but with significantly different growth rates. First-principles calculation results show that the epitaxial nucleation of the second graphene layer is mainly due to the active CH_3 radicals and the Cu substrate with a covered graphene layer. We believe that we have uncovered a new territory in the CVD nucleation mechanism of epitaxial graphene growth, and hope that this understanding will bring the advent of CVD graphene growth with more precise control of radicals in the future.

Experimental section

BLG synthesis

BLG was synthesized by low-pressure CVD using bubbled ethanol. Commercially available Cu foil (25 μm thick, #46365,

Fig. 5 (a) Decomposition products of CH_i radicals from C_2H_5OH and CH_4 at 1000 °C, calculated by CHEMKIN-II. (b) The relative Gibbs free energies of species of each CH_i radical on Cu(111)/MLG as a function of the chemical potential of H.

Alfa Aesar China Chemical Co., Ltd) was used as received. A flat Cu foil was placed in a hot-wall CVD quartz chamber (i.d. = 60 mm), and annealed at 1000 °C for 30 minutes with 100 sccm H_2, followed by introducing a 20 sccm Ar/ethanol mixture gas. H_2 was stopped at the growth step of graphene. After growth, the chamber was slowly cooled to room temperature at a rate of 10–20 °C min^{-1}.

Graphene transfer

BLG film on copper was firstly coated with polymethylmethacrylate (PMMA, 4 wt% in anisole) by the spin-coating method, and baked on a hotplate at 140 °C for 30 min. The graphene film on the other side of the Cu foil was treated by O_2 plasma (100 W) for 30 s. The Cu substrate was then etched away in 1 M $FeCl_3$ solution and the PMMA/graphene film was rinsed in DI water 3 times and transferred onto the Si/SiO$_2$ substrate. Finally, the PMMA layer was removed by hot acetone.

Characterization

Characterization of as-grown and transferred BLG was carried out by optical microscopy (Olympus BXFM-ILHS, Olympus Co., Ltd), scanning electron microscopy (SEM, 5 kV, S-3400, Hitachi Co., Ltd), confocal micro-Raman spectroscopy (LabRAM HR Evolution, Horiba Co., Ltd), and transmission electron microscopy (JEM-2100, JEOL Co., Ltd).

First-principles calculations

The first-principles calculations are performed with the density-functional theory approach as implemented by the Vienna *ab initio* Simulation Package (VASP).[33,34] The exchange–correlation energy is treated in the Perdew–Burke–Ernzerhof (PBE) version of the generalized-gradient approximation (GGA) functional.[35,36] In order to accurately describe the vdWs between a CH_i (i = 0, 1, 2, 3) radical and the Cu surface, the PBE functional with the vdWs correction (DFT-D3)[37] has also been used. The energy cutoff of the plane-wave expansion is set at 400 eV. All structures are optimized by the conjugate gradient method until the forces acting on each atom are less than 0.01 eV Å^{-1}. Cu(111) surfaces are modelled using slab geometry with four metal atomic layers in which the bottom-layer atoms are fixed at their respective bulk positions. For the geometry optimization, all atoms except for the fixed bottom-layer atoms are fully relaxed and then various CH_i species are put on the metal substrate surface for further optimization.

Ethanol decomposition simulation

Simulation of ethanol decomposition was performed using SENKIN,[38,39] a computer program that predicts the time-dependent chemical-kinetic behaviour of a homogeneous gas mixture in a closed system. This has been incorporated into CHEMKIN-II,[40] which is a package of computer codes for the analysis of gas-phase chemical kinetics. Constant-temperature and constant-pressure conditions were chosen for the calculations using temperatures and pressures that had been experimentally found to be optimum for BLG growth.

Acknowledgements

References

1 Y. Zhang, T.-T. Tang, C. Girit, Z. Hao, M. C. Martin, A. Zettl, M. F. Crommie, Y. R. Shen and F. Wang, *Nature*, 2009, **459**, 820–823.

2 K. F. Mak, C. H. Lui, J. Shan and T. F. Heinz, *Phys. Rev. Lett.*, 2009, **102**, 256405.

3 X. S. Li, W. W. Cai, J. H. An, S. Kim, J. Nah, D. X. Yang, R. Piner, A. Velamakanni, I. Jung, E. Tutuc, S. K. Banerjee, L. Colombo and R. S. Ruoff, *Science*, 2009, **324**, 1312–1314.

4 S. Bae, H. Kim, Y. Lee, X. Xu, J.-S. Park, Y. Zheng, J. Balakrishnan, T. Lei, H. Ri Kim, Y. I. Song, Y.-J. Kim, K. S. Kim, B. Ozyilmaz, J.-H. Ahn, B. H. Hong and S. Iijima, *Nat. Nanotechnol.*, 2010, **5**, 574–578.

5 Y. Hao, M. S. Bharathi, L. Wang, Y. Liu, H. Chen, S. Nie, X. Wang, H. Chou, C. Tan, B. Fallahazad, H. Ramanarayan, C. W. Magnuson, E. Tutuc, B. I. Yakobson, K. F. McCarty, Y.-W. Zhang, P. Kim, J. Hone, L. Colombo and R. S. Ruoff, *Science*, 2013, **342**, 720–723.

6 S. Lee, K. Lee and Z. Zhong, *Nano Lett.*, 2010, **10**, 4702–4707.

7 Z. Sun, A.-R. O. Raji, Y. Zhu, C. Xiang, Z. Yan, C. Kittrell, E. L. G. Samuel and J. M. Tour, *ACS Nano*, 2012, **6**, 9790–9796.

8 H. Zhou, W. J. Yu, L. Liu, R. Cheng, Y. Chen, X. Huang, Y. Liu, Y. Wang, Y. Huang and X. Duan, *Nat. Commun.*, 2013, **4**, 2096.

9 H.-B. Sun, J. Wu, Y. Han, J.-Y. Wang, F.-Q. Song and J.-G. Wan, *J. Phys. Chem. C*, 2014, **118**, 14655–14661.

10 Q. Li, H. Chou, J.-H. Zhong, J.-Y. Liu, A. Dolocan, J. Zhang, Y. Zhou, R. S. Ruoff, S. Chen and W. Cai, *Nano Lett.*, 2013, **13**, 486–490.

11 W. Fang, A. L. Hsu, R. Caudillo, Y. Song, A. G. Birdwell, E. Zakar, M. Kalbac, M. Dubey, T. Palacios, M. S. Dresselhaus, P. T. Araujo and J. Kong, *Nano Lett.*, 2013, **13**, 1541–1548.

12 J. K. Wassei, M. Mecklenburg, J. A. Torres, J. D. Fowler, B. C. Regan, R. B. Kaner and B. H. Weiller, *Small*, 2012, **8**, 1415–1422.

13 K. Yan, H. Peng, Y. Zhou, H. Li and Z. Liu, *Nano Lett.*, 2011, **11**, 1106–1110.

14 L. Liu, H. Zhou, R. Cheng, W. J. Yu, Y. Liu, Y. Chen, J. Shaw, X. Zhong, Y. Huang and X. Duan, *ACS Nano*, 2012, **6**, 8241–8249.

15 P. Zhao, S. Kim, X. Chen, E. Einarsson, M. Wang, Y. Song, H. Wang, S. Chiashi, R. Xiang and S. Maruyama, *ACS Nano*, 2014, **8**, 11631–11638.

16 L. M. Malard, M. A. Pimenta, G. Dresselhaus and M. S. Dresselhaus, *Phys. Rep.*, 2009, **473**, 51–87.

17 Z. Peng, Z. Yan, Z. Sun and J. M. Tour, *ACS Nano*, 2011, **5**, 8241–8247.

18 Z. H. Ni, Y. Y. Wang, T. Yu, Y. M. You and Z. X. Shen, *Phys. Rev. B: Condens. Matter*, 2008, **77**, 235403.

19 H. Shu, X.-M. Tao and F. Ding, *Nanoscale*, 2015, **7**, 1627–1634.

20 C. T. Rettner, E. K. Schweizer and H. Stein, *J. Chem. Phys.*, 1990, **93**, 14442.

21 L. Mandeltort, P. Choudhury, J. K. Johnson and J. T. Yates, *J. Phys. Chem. Lett.*, 2012, **3**, 1680–1683.

22 A. H. Castro Neto, F. Guinea, N. M. R. Peres, K. S. Novoselov and A. K. Geim, *Rev. Mod. Phys.*, 2009, **81**, 109–162.

23 B. Hou, R. Xiang, T. Inoue, E. Einarsson, S. Chiashi, J. Shiomi, A. Miyoshi and S. Maruyama, *Jpn. J. Appl. Phys.*, 2011, **50**, 065101.

24 R. Xiang, B. Hou, E. Einarsson, P. Zhao, S. Harish, K. Morimoto, Y. Miyauchi, S. Chiashi, Z. Tang and S. Maruyama, *ACS Nano*, 2013, **7**, 3095–3103.

25 J. Park, R. S. Zhu and M. C. Lin, *J. Chem. Phys.*, 2002, **117**, 3224–3231.

26 J. Li, A. Kazakov and F. L. Dryer, *J. Phys. Chem. A*, 2004, **108**, 7671–7680.

27 R. Sivaramakrishnan, M. C. Su, J. V. Michael, S. J. Klippenstein, L. B. Harding and B. Ruscic, *J. Phys. Chem. A*, 2010, **114**, 9425–9439.

28 Z. F. Xu, K. Xu and M. C. Lin, *J. Phys. Chem. A*, 2011, **115**, 3509–3522.

29 R. Wellmann, A. Böttcher, M. Kappes, U. Kohl and H. Niehus, *Surf. Sci.*, 2003, **542**, 81–93.

30 P. Zhao, A. Kumamoto, S. Kim, X. Chen, B. Hou, S. Chiashi, E. Einarsson, Y. Ikuhara and S. Maruyama, *J. Phys. Chem. C*, 2013, **117**, 10755–10763.

31 K. May, S. Dapprich, F. Furche, B. V. Unterreiner and R. Ahlrichs, *Phys. Chem. Chem. Phys.*, 2000, **2**, 5084.

32 L. K. Rutz, H. Bockhorn and J. W. Bozzelli, *Abstr. Pap. Am. Chem. Soc.*, 2004, **227**, U1100–U1101.

33 P. E. Blöchl, *Phys. Rev. B: Condens. Matter*, 1994, **50**, 17953–17979.

34 G. Kresse and J. Furthmüller, *Phys. Rev. B: Condens. Matter*, 1996, **54**, 11169–11186.

35 J. P. Perdew, K. Burke and M. Ernzerhof, *Phys. Rev. Lett.*, 1996, **77**, 3865–3868.

36 G. Kresse and D. Joubert, *Phys. Rev. B: Condens. Matter*, 1999, **59**, 1758–1775.

37 S. Grimme, S. Ehrlich and L. Goerigk, *J. Comput. Chem.*, 2011, **32**, 1456–1465.

38 A. Varykhalov, J. Sanchez-Barriga, A. M. Shikin, C. Biswas, E. Vescovo, A. Rybkin, D. Marchenko and O. Rader, *Phys. Rev. Lett.*, 2008, **101**, 157601.

39 Y. Murata, V. Petrova, B. B. Kappes, A. Ebnonnasir, I. Petrov, Y. H. Xie, C. V. Ciobanu and S. Kodambaka, *ACS Nano*, 2010, **4**, 6509–6514.

40 R. Q. Zhao, Y. F. Zhang, T. Gao, Y. B. Gao, N. Liu, L. Fu and Z. F. Liu, *Nano Res.*, 2011, **4**, 712–721.